Mem. S.A.It. Vol. 84, 1142

Memorie della

Linear polarization of rapidly rotating ultracool dwarfs

P. A. Miles-Páez[1,2], M. R. Zapatero Osorio[3], E. Pallé[1,2], P. Montañés-Rodríguez[1,2], and K. Peña Ramírez[1,2]

[1] Instituto de Astrofísica de Canarias, La Laguna, E38205 Spain
e-mail: pamp@iac.es
[2] Departamento de Astrofísica, Universidad de La Laguna, La Laguna, Spain
[3] Centro de Astrobiología, CSIC-INTA, Madrid, Spain

Abstract. We present imaging linear polarimetry data of a sample of 18 late-M, L-, and early-T type dwarfs taken with the *Z*- and *J*-band filters and the LIRIS instrument of the 4.2-m William Herschel Telescope. All of our targets have projected rotational velocities $\geq$ 30 km s^{-1} and oblate ultracool atmospheres ($T_{\rm eff}$ < 2700 K), which may harbor clouds of condensate particles. Our polarimetric measurements have typical error bars of ±0.13%, i.e., linear polarization degrees larger than 0.4% can be detected with a confidence of $\geq 3\sigma$. Seven dwarfs appear to be polarized in the *J*-band with indices of P = 0.4–0.7%, suggesting the presence of atmospheric dusty structures. There is a hint that the dwarfs with the largest rotations ($v \sin i \geq 60$ km s^{-1}) show higher incidence of detected *J*-band linear polarization than the dwarfs with smaller projected rotational velocities. We also detect linear polarization variability indicative of "weather".

Key words. polarization – brown dwarfs – stars: atmospheres – stars: late-type – stars: low-mass

1. Introduction

Dwarfs with spectral types cooler than M7 ($T_{\rm eff} \leq 2700$ K; typically referred to as ultracool dwarfs) are believed to undergo the formation of a wide range of atmospheric condensate species (solid and liquid particles) such as corundum (Al_2O_3), iron (Fe), enstatite ($MgSiO_3$), forsterite (Mg_2SiO_4), titanium dioxide (TiO_2), and gehlenite ($Ca_2Al_2SiO_7$) among others (Jones & Tsuji 1997; Ackerman & Marley 2001; Helling et al. 2008; Witte et al. 2011). According to models, these condensates may build up into structures (e.g., "clouds"), which are located in the outer layers of the atmosphere for $T_{\rm eff} \geq$1300 K and in layers below the visible photosphere for $T_{\rm eff} \lesssim$1300 K (Allard et al. 2001). Condensates or "dusty particles" represent one relevant and yet poorly understood source of opacity in ultracool dwarfs. Atmospheric dust may also polarize the object's output light at particular wavelengths through scattering processes as suggested by the theoretical work of Sengupta & Krishan (2001), and observationally demonstrated by the detection of linear polarization at optical and near-infrared frequencies (Ménard et al. 2002; Zapatero Osorio et al.

Send offprint requests to: P. A. Miles-Páez

2005; Goldman et al. 2009; Tata et al. 2009; Zapatero Osorio et al. 2011). Polarization may become a useful tool to comprehend the complexity of ultracool atmospheres.

Additionally, ultracool dwarfs have high values of projected rotational velocities ($v \sin i$) indicating that they are indeed rapid rotators (Zapatero Osorio et al. 2006; Konopacky et al. 2012, and references therein).

This fact combined with convection and the presence of dust could give rise to intricate atmospheric dynamics, likely generating periodic and non-periodic photometric variability as seen in some late-M, L, and T dwarfs (Bailer-Jones & Mundt 2001; Martín et al. 2001; Koen 2004; Buenzli et al. 2012).

From a theoretical perspective, Sengupta & Krishan (2001), Sengupta (2003), Sengupta & Kwok (2005), Sengupta & Marley (2010), and de Kok et al. (2011) predicted that ultracool dwarfs with atmospheric condensates and high $v \sin i$'s show measurable linear polarization degrees of typically $\lesssim 1\%$ in the optical and near-infrared. Fast rotation makes dwarf to take the shape of an oblate ellipsoid, and this lack of symmetry leads to incomplete cancellation of the polarization from different areas of the surface. Gravity is an additional ingredient to take into account since rotationally induced non-sphericity is favored at lower atmospheric gravities. For a similar amount of dust particles in the ultracool atmospheres it is expected that the largest rotations and lowest gravities produce the largest polarization degrees.

Here, we aim at studying the capabilities of linear polarization in the near infrared to probe the presence of atmospheric condensates in ultracool dwarfs and to shed new light on the dependence of the linear polarization with rotation. The results shown in this proceeding have been recently accepted for publication (Miles-Páez et al. 2013).

2. Target selection and observations

We selected 18 bright ($10.3 < J < 14.9$ mag) ultracool dwarfs with spectral types from M7 through T2 and published projected rotational velocities $v \sin i \geq 30$ km s^{-1} (Zapatero Osorio et al. 2006; Konopacky et al. 2012, and references therein). All dwarfs are observable from northern astronomical observatories and sufficiently bright at near-infrared wavelengths to achieve accurate polarimetric photometry ($\sigma \leq 0.2\%$) using short exposures and 4-m class telescopes. They represent $\sim 37\%$ of all dwarfs cooler than M7 that have $v \sin i \geq 30$ km s^{-1} available in the literature (see Figure 1). In Table 1, we provide the targets complete names and their spectral types.

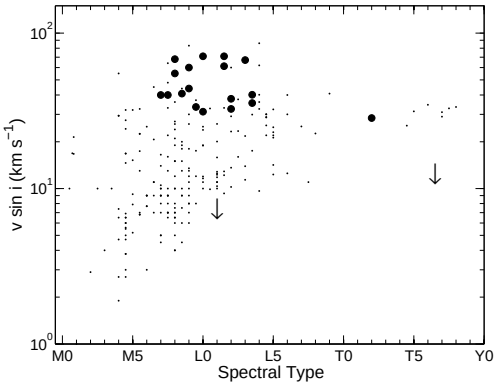

Fig. 1. Projected rotational velocity ($v \sin i$) as a function of spectral type. Our sample of fast rotators is shown with black circles while literature objects are shown in black dots. Error bars are not shown for the clarity of the figure, arrows show upper limits. Data taken from Konopacky et al. (2012); Zapatero Osorio et al. (2006) and references therein.

We carried out several linear polarimetric campaigns using the Z and J-bands filter and LIRIS on the 4.2–m William Herschel Telescope in La Palma island (Spain). In Table 1, we provide the filters and dates of observations for each target. These were observed following a nine–point dither pattern for a proper sky background contribution removal. Typical individual exposure times were in the range 5–180 s depending on the target's brightness, filter and seeing.

In its polarimetric imaging mode, LIRIS uses a Wedged double Wollaston device, consisting in a combination of two Wollaston prisms that deliver four simultaneous images of the polarized flux at vector angles 0° and 90°, 45° and 135°. Raw data frames were divided into four slices corresponding to the po-

Table 1. Targets and linear polarization measurements

Name	SpT	Fil	Obs. date (JD-2450000.5)	p^* (%)	Θ (deg)
2MASS J00192626+4614078	M8	*J*	6206.8719	0.38 ± 0.15	–
		Z	6207.9954	0.57 ± 0.13	146.8 ± 6.7
BRI 0021−0214	M9.5	*J*	6206.8988	0.09 ± 0.11	–
LP 349−25AB	M8+M9	*J*	6206.9830	0.18 ± 0.11	–
		Z	6208.4696	0.20 ± 0.10	–
2MASS J00361617+1821104	L3.5	*J*	6207.0147	0.20 ± 0.11	–
2MASS J00452143+1634446	L2	*J*	6207.0275	0.00 ± 0.11	–
2MASS J02281101+2537380	L0	*J*	6207.0697	0.35 ± 0.14	–
LP 415−20AB	M7+M9.5	*J*	6207.2099	0.39 ± 0.12	174.9 ± 9.0
		Z	6208.2221	0.38 ± 0.12	176.3 ± 9.4
2MASS J07003664+3157266AB	L3.5+L6	*J*	6207.2425	0.48 ± 0.14	87.3 ± 7.8
2MASS J08283419−1309198	L2	*J*	5927.1754	0.14 ± 0.10	–
		J	6321.0538	0.22 ± 0.15	–
2MASS J11593850+0057268	L0	*J*	6094.9304	0.53 ± 0.15	28.3 ± 8.0
		J	6321.1119	0.40 ± 0.13	179.0 ± 9.0
2MASS J12545393−0122474	T2	*J*	6321.1575	0.00 ± 0.34	–
2MASS J14112131−2119503	M9	*J*	6094.9835	0.48 ± 0.17	148.7 ± 10.0
2MASS J15010818+2250020	M9	*J*	6321.1950	0.51 ± 0.12	46.2 ± 7.0
2MASS J15210103+5053230	M7.5	*J*	6321.2133	0.60 ± 0.13	13.8 ± 6.2
2MASS J18071593+5015316	L1.5	*J*	6094.1371	0.67 ± 0.11	67.0 ± 5.0
		Z	6207.8720	0.15 ± 0.15	–
2MASS J18353790+3259545	M8.5	*J*	6094.1755	0.07 ± 0.10	–
2MASS J20360316+1051295	L3	*J*	6094.1880	0.18 ± 0.16	–
		Z	6207.9429	0.73 ± 0.28	–
2MASS J20575409−0252302	L1.5	*J*	6206.8253	0.40 ± 0.15	–

larimetric vectors, and each slice was reduced following standard procedures for the near infrared (sky substraction, flat-field correction, alignment and combination of the nine images of the pattern).

3. Results and discussion

Linear polarization degrees and polarization angles were derived from the Stokes parameters as explained in Zapatero Osorio et al. (2011). The *J* magnitudes of the fast rotators sample are in the range 10.3-14.1 mag, which provide enough photons to reach accuracies of $\sim \pm 0.13\%$ in the *Z* and *J* linear polarimetric measurements. According to the 3σ criterion, $P/\sigma \geq 3$ (P and σ are linear polarization degree and its associated uncertainty), we can detect polarimetric signals with indices higher than $P = 0.4\%$. About 40% of our sample (7 out of 18 sources in the *J*-band, and 2 out of 5 in the *Z* filter) appear to be linearly polarized.

Because the linear polarization degree P is always a positive quantity, small values of P and values of P affected by poor signal-to-noise-ratio data are statistically biased toward an overestimation of the true polarization. We applied the equation given by Wardle & Kronberg (1974) to derive the debiased linear polarization degree, p^*, by taking into account the measured P and its associated uncertainty:

$$p^* = \sqrt{P^2 - \sigma^2} \quad (1)$$

The debiased linear polarization degree (p^*) and the polarization vibration angle (Θ) are provided in Table 1.

3.1. Linear polarization versus rotation

In Figure 2, we plotted the degree of linear polarization in the *J* (left) and *Z* (right) bands as

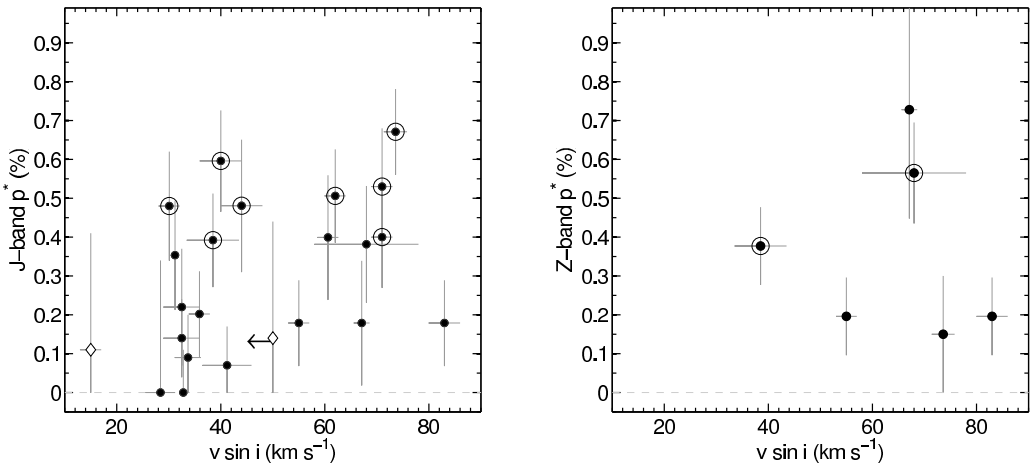

Fig. 2. *Z*-band (right) and *J*-band (left) degree of linear polarization as a function of $v \sin i$ for our sample of fast rotators. Polarized objects (i.e., $P/\sigma \geq 3$) are plotted as encircled symbols. Diamonds are objects taken from Zapatero Osorio et al. (2011), the arrow shows the upper limit for $v \sin i$.

a function of the projected rotational velocity ($v \sin i$) for the fast rotators sample. We have included two objects from Zapatero Osorio et al. (2011), which were observed using the same instrumental configuration. From the *J*-band data, we find that the fraction of polarized objects for $v \sin i \geq 60\,\mathrm{km\,s^{-1}}$ is nearly a factor 2 larger than the fraction of polarized objects with $v \sin i = 30$–$60\,\mathrm{km\,s^{-1}}$. *Z*-band data are consistent with the *J*-band data. Numbers are still low and more measurements are needed to perform more robust statistics.

To minimize the uncertainty introduced by the inclination angle of the spin axis in $v \sin i$, we plot the polarimetric measurements as a function of rotation period in Figure 3. Rotation periods have been obtained from the literature for a total of 6 objects in the full sample. We note that all these sources are field dwarfs (e.g., they likely have metal abundance close to solar), and none is reported to be exceptionally young, so they are expected to have a similar size of about one Jupiter radius (Baraffe et al. 2003). Theory suggests that fast rotations favor the detection of polarization. In Figure 3 the only polarized object is that with the shortest rotation period or the largest $v \sin i$, however there are too few data to make solid conclusions on the role of rotation in the detection of polarization.

3.2. Time variability of the linear polarization

We investigated the variability of the linear polarization degree for objects with measurements available on different occasions. We find that both the degree of linear polarization (P) and the vibration angle of the polarization (Θ) remain almost constant (within the error bars) in consecutive measurements separated by a day or $\sim$ 20 rotations (assuming $v_{\rm rot} = 60\,\mathrm{km\,s^{-1}}$ and size $1\,R_{Jup}$).

However, when comparing measurements of the same object taken in the same filter, using the same instrumental configuration but separated by several months (or a few thousands rotation cycles), P and Θ varies. We attribute this to changes in the dusty cloud patterns of the atmospheres likely due to rapid rotation and convective motions (Showman & Kaspi 2013; de Kok et al. 2011).

4. Conclusions

About 40±15% of rapidly rotating, field M7-L3.5 dwarfs show significant linear polarization at 1.25 μm with degrees in the interval $p^* \sim 0.4$–0.8%, in agreement with published theoretical models.

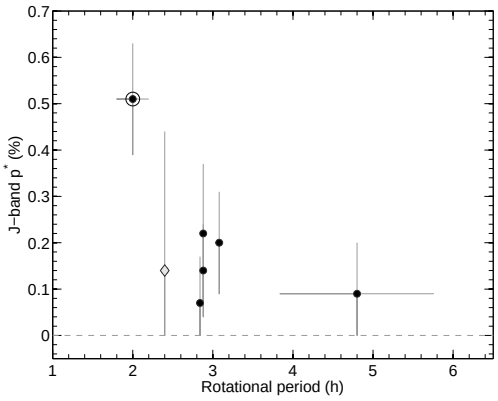

Fig. 3. *J*-band degree of linear polarization as a function of the rotation period. Polarized objects are plotted as encircled symbols. Diamonds stand for objects taken from Zapatero Osorio et al. (2011).

Also, we find that linear polarimetric measurements are stable over periods of a few days or a few tens rotation cycles. However, they change dramatically over periods of a few months or thousands rotation cycles. We attribute these variations to changes in the clouds due to rotation and convection.

Acknowledgements. The William Herschel Telescope is operated on the island of La Palma by the Isaac Newton Group in the Spanish Observatorio del Roque de los Muchachos of the Instituto de Astrofísica de Canarias. This research has made use of NASA Astrophysics Data System and the SIMBAD database. Also, this publication makes use of data products from the Wide-field Infrared Survey Explorer. This work is partly financed by the Spanish Ministry of Economics and Competitiveness through projects AYA2010-21308-C03- 02 and AYA2011-30147-C03-03.

References

Ackerman, A. S., & Marley, M. S. 2001, ApJ, 556, 872
Allard, F., et al 2001, ApJ, 556, 357
Bailer-Jones, C. A. L., & Mundt, R. 2001, A&A, 367, 218
Baraffe, I., et al. 2003, A&A, 402, 701
Buenzli, E., et al. 2012, ApJ, 760, L31
Cruz, K. L., Kirkpatrick, J. D., & Burgasser, A. J. 2009, AJ, 137, 3345
de Kok, R. J., Stam, D. M., & Karalidi, T. 2011, ApJ, 741, 59
Goldman, B., Pitann, J., Zapatero Osorio, M. R., et al. 2009, A&A, 502, 929
Helling, C., et al. 2008, MNRAS, 391, 1854
Jones, H. R. A., & Tsuji, T. 1997, ApJ, 480, L39
Koen, C. 2004, MNRAS, 354, 378
Konopacky, Q. M., et al. 2012, ApJ, 750, 79
Marley, M. S., & Sengupta, S. 2011, MNRAS, 417, 2874
Martín, E. L., Zapatero Osorio, M. R., & Lehto, H. J. 2001, ApJ, 557, 822
Ménard, F., Delfosse, X., & Monin, J.-L. 2002, A&A, 396, L35
Miles-Páez, P. A., Zapatero Osorio, M. R., Pallé, E., & Peña Ramírez, K. 2013, A&A, 556, 125.
Sengupta, S. 2003, ApJ, 585, L155
Sengupta, S., & Krishan, V. 2001, ApJ, 561, L123
Sengupta, S., & Kwok, S. 2005, ApJ, 625, 996
Sengupta, S., & Marley, M. S. 2009, ApJ, 707, 716
Sengupta, S., & Marley, M. S. 2010, ApJ, 722, L142
Showman, A. P., & Kaspi, Y. 2013, ApJ, 776, 85
Tata, R., et al. 2009, A&A, 508, 1423
Wardle, J. F. C., & Kronberg, P. P. 1974, ApJ, 194, 249
Witte, S., et al. 2011, A&A, 529, A44
Zapatero Osorio, M. R., Caballero, J. A., & Béjar, V. J. S. 2005, ApJ, 621, 445
Zapatero Osorio, M. R., et al. 2006, ApJ, 647, 1405
Zapatero Osorio, M. R., et al. 2011, ApJ, 740, 4